PERIODICO di MINERALOGIA
established in 1930

Dipartimento
di Scienze della Terra
Sapienza
Università di Roma

An International Journal of
Mineralogy, Crystallography, Geochemistry,
Ore Deposits, Petrology, Volcanology
and applied topics on Environment, Archaeometry and Cultural Heritage

Petrography and mineralogical study of gold mineralization in the Tasiast Archean deposits (Mauritania)

Mesbaha Zeine [1], Samir Mefteh [1], Jean-Marc Baele [2], Joris Coron [2], Séverine Papier [2], Ahmed Hamoud [3], Mounir Medhioub [1,*]

[1] Laboratory of Spectroscopic Characterization and Optical Materials (LaSCOM), University of Sfax, Faculty of Sciences, B.P. 1171, 3000, Tunisia
[2] Department of Geology, Faculty of Engineering, University of Mons, 7000 Mons, Belgium
[3] Department of Geology, Faculty of Sciences and Technics, University of Nouakchott Al-Aasriya, Mauritania

ARTICLE INFO

Submitted: November 2024
Accepted: January 2025
Available on line: January 2025

* Corresponding author:
mounirmedhioub@yahoo.fr

Doi: 10.13133/2239-1002/18697

How to cite this article:
Zeine M. et al. (2025)
Period. Mineral. 94, 1-20

ABSTRACT

This study aims to determine the mineral phases containing gold mineralization and other mineral indicators in two prominent deposits (West Branch and Piment) in Tasiast. This latter area is one of the major areas of the Reguibat Shield and is primarily composed of Mesoarchean rocks from the Aoueouat greenstone belt. In addition, the West Branch is hosted in meta-igneous rocks, whereas Piment is situated within meta- sedimentary rocks. The results of 55 samples collected from the cores of two boreholes show that the crossed series is composed by rocks of the types felsite (FVC), greywacke (SGW), siltstone (SVC), micaschist (MCS) and banded iron formation (BIF). Petrographic observations via polished and thin sections, scanning electron microscopy (SEM) and cathodoluminescence (CL) confirmed by mineralogical results were performed by means X-ray diffraction (XRD), revealed that the genesis of gold deposits in both boreholes was linked mainly to hydrothermal activity.

The minerals associated with the hydrothermal deposits are biotite, muscovite, fuchsite, zoisite, staurolite, chlorite, cummingtonite, tourmaline, hornblende and garnet. They are present in variable proportions in the crossed rocks, which suffered a high degree of metamorphism. On the other hand, the genesis of gold is mostly linked to hydrothermal activity. In fact, this mineral is associated mainly with sulfides such as pyrrhotite and occasionally appears as inclusions inside pyrite and arsenopyrite. Therefore, the hydrothermal system that generated the gold mineralization was likely active under brittle and ductile deformation conditions after mild metamorphism.

Keywords: Tasiast deposits; Archean; petrography; mineralogy; gold mineralization; hydrothermalism; metamorphism.

INTRODUCTION

Mauritania is rich in natural resources such as gold, iron, gypsum, quartz, salt, copper and crude oil (Heron et al., 2016; Eglinger et al., 2023). In 2017, it was ranked as the second African country in terms of iron export (Sabeima et al., 2024). For several years, it has been a target for gold exploration and mining by the world's leading mining companies because of its world-class gold deposits. The gold reserves of Mauritania include 25 million ounces, reported as 780 metric tons (Taib, 2019; Bhuiyan et al., 2022). This interest has triggered the development of a large number of scientific studies and industrial projects among international geological surveys and mining companies. It's also led to the detection of high-potential gold mineralization zones and the discovery of numerous gold deposits. In addition, gold deposits are located mainly in the Archean formations of the Reguibat Shield in the Tasiast deposit (Dosso et al., 1979; Montero et al., 2014; Aïfa, 2021; Jiang et al., 2022; Mahmoud et al., 2023). The Tasiast mine is the largest open-pit gold mine in West Africa (Mykhailov et al., 2023; Zeine et al., 2022; Trench, 2024), it is composed of Archean terrains older than 2.5 Ga (Chardon, 1996; Key et al., 2008; Schofield et al., 2012; Mignot et al., 2014; Markwitz et al., 2016a; El Abd Bouha et al., 2021) and that are situated in the Reguibat ridge, one of Mauritania's five main geological formations. In addition, it contains greenstone belts that have major economic significance around the world due to the presence of a variety of natural resources, including gold deposits (Montero et al., 2014; Markwitz et al., 2016b; Hamimi et al., 2024). Therefore, by the end of 2018, this mine had produced a total of approximately 2.2 million ounces of gold since it first started operating commercially in 2010 by Kinross Gold Corporation (Sims, 2019). On the other hand, in greenstone and Archean granitoid terrains, shear-hosted gold deposits exhibit structural and lithological control over gold mineralization, so they are crucial for localizing gold deposits (Higashihara et al., 2004; Goldfarb et al., 2017; Amadu et al., 2021; Ouattara et al., 2021; Tan et al., 2022). Consequently, to understand lithological and structural controls, this study uses complementary approaches, including mining data, petrographic and mineralogical surveys as part of the metallogenic investigation of the Tasiast deposit. As well, this study aimed to ascertain the degree of alteration and the phenomena associated with the precipitation of mineralization, both of which can be used as model guides for exploration efforts in order to search and prospect for new gold deposit domains.

The approach of this study is essentially based on the inventory of rock series constituting the belt of greenstone rocks crossed by mining surveys in the two sectors of Piment and West Branch. Against this background, the present study aims to (i) identify the mineralogical associations of the collected samples in a detailed and systematic manner (for the purpose of detecting hydrothermal alteration products (minerals with evidence of alteration) and determining their type); (ii) understand the main structural relationships between different constituents of minerals and their surface state, especially in terms of transformation; (iii) detect possible anomalies indicative of mineralization and understand the mechanisms responsible for the enrichment of this gold mineralization in its tectonic (geo-structural) framework; and (iv) compare the two sectors and synthesize the paragenetic sequence to establish the genesis of gold mineralization.

GEOLOGICAL STRUCTURE OVERVIEW AND GOLD MINERALIZATION PROCESS

The Tasiast mine is located in the northwest of Mauritania, approximately 300 km in the north of the country's capital Nouakchott (Figure 1). In addition, Tasiast is a part of the northern region of the west African craton, which corresponds to the Reguibat Shield. This latter is one of the five main geological units in Mauritania and spans more than 1500 km in length and 400 km in width. The Reguibat Shield has been divided into two main sections (Bessoles, 1977; Vachette et al., 1973): (i) Amsaga, Tijirit, Tiris, Tasiast, Ouassat, Ghallaman, and Sfariat types of gneiss, which are dated at ≈3.5 Ga (Potrel et al., 1996) and have tectono-magmatic phases of ≈3.3, ≈3.0, and ≈2.7 Ga (Potrel et al., 1998), and (ii) the Yeti and Eglab chains in central and eastern Mauritania are part of a Paleoproterozoic belt that consists mostly of granitoids formed between 2.2 Ga and 2.1 Ga and associated with some remnants of Archean oceanic crust that were dated at 2.7 Ga (Boher et al., 1990) (Figure 2). In addition, this belt consists of two major subdivisions separated by a crust-scale shear zone that serves as a major accretion boundary (Lahondère et al., 2003; Schofield et al., 2006). The rocks of the first belt are represented by granitoid-gneissic complexes, which include basic and ultrabasic rocks with metamorphosed sediments and potassium-rich granitoid. These metamorphic terrains are abundantly exposed in Amsaga (Blanchot, 1955; Barrère, 1967; Haissen et al., 2017; Ishagh et al., 2021). The secondary belt is composed by Mesoarchean to Paleoproterozoic rocks in the southwest, where the Tasiast deposits are found, including high-grade granite gneiss and greenstone belt assemblages. More precisely, the Tasiast deposit is situated within the Aoueouat Archean greenstone belt, where gold mineralization is observed within the supracrustal belt, characterized by distinct attributes such as prominent foliation and closely folded isoclinal structures, which are primarily oriented in a north–south direction (Heron et al., 2016; Sims, 2019). Furthermore, ultramafic, mafic, and felsic volcanic and intrusive rocks, as well as sedimentary rocks and banded iron formations, are all part of the supracrustal succession. Moreover, the Aoueouat greenstone belt units have undergone metamorphism from the lower amphibolite facies to the middle-greenschist. The hanging wall of the local west-converging Tasiast thrust fault system is where gold mineralization is thought to have occurred. On the other hand, deposits are commonly located in second or third-order structures, predominantly near large scale compressional structures. The controlling structures are typically ductile to brittle and highly variable in type.

However, the gold endowment of the brittle-ductile shear zones is related to the interplay of several factors:

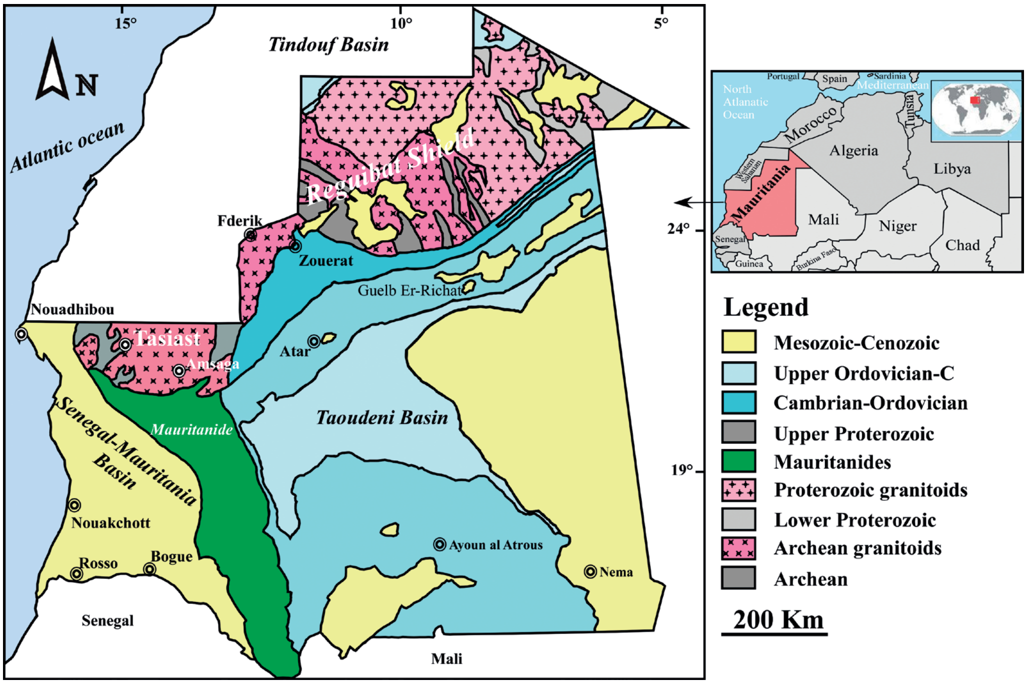

Figure 1. Structural domains of Mauritania (Bradley et al., 2015 in Hamoud et al., 2021; modified).

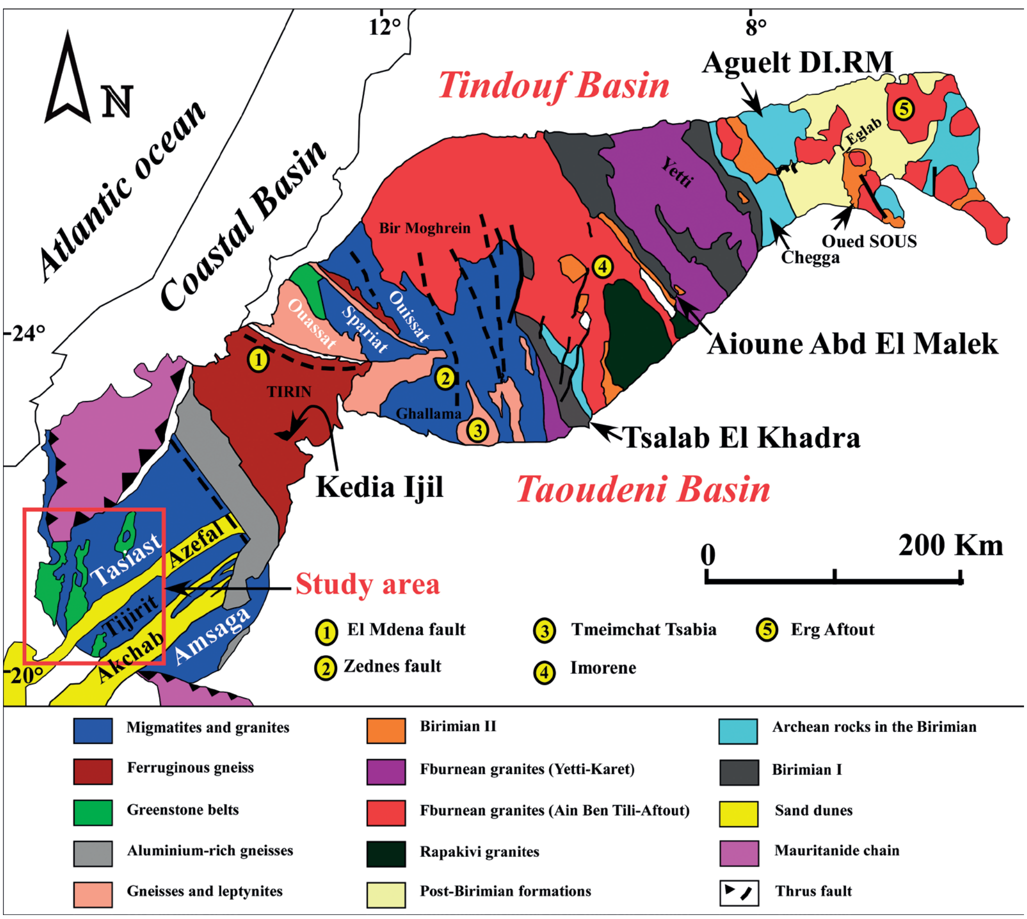

Figure 2. Geological map of the Reguibat Shield and lithostratigraphic Units (Bronner et al., 1992; modified).

the first is related to the extreme lithologic competency contrasts that lead to more heterogeneous fluid flow; the second is due to the degree of straining of the rock package, exemplified by the attenuation of the stratigraphy; the third factor is the metamorphic facies, particularly its role in the volume of infiltrating fluids (Phillips et al., 1996; Moussa Hamath et al., 2020); the fourth is due to the rock permeability (Manning and Ingebritsen, 1999); and the fifth factor is related to the variety of orientations of lithological contacts and structures giving rise to zones of dilation. In addition, shear zones in which fluids flow with little perturbation, including highly attenuated/sheared rocks metamorphosed in amphibolite facies with little angular discordance, should be assigned low exploration priority. On the other hand, greenschist facies shear zones with various orientations of lithological contacts and structures, various lithologies, and close proximity to regional seals should be assigned the highest priorities (Weinberg et al., 2004).

The vein morphology and quartz textures indicate intense sinistral shearing, suggesting synkinematic mineralization. Carbonitization, sulfidation, and chloritization are the dominant hydrothermal alteration styles, with refractory gold present in arsenopyrite and As-rich pyrite, which is typical for orogenic gold deposits (Groves et al., 1998, 2003). Additionally, inclined stretching lineations and slickensides in silicified shear zones on vein walls and shallow dips of extensional veins attest to their formation during crustal shortening (Sibson et al., 1988; Witt et al., 1998; Robert and Poulsen, 2001). These orogenic gold deposits have consistent spatial and temporal positions and formed during deformational processes at convergent margins independently of the age of the host rock, which can include both Archean and Proterozoic greenstone belts (Mikucki et al., 1993; Phillips et al., 1996).

MATERIALS AND METHODS

The integration of field work, drilling, mining data and laboratory analyses consisted of identifying demarcated areas with gold mineralization and collecting samples for mineralogical analysis and petrographic descriptions.

Therefore, two diamond drill cores were chosen (Figure 3) from multiple diamond core drillings within the primary shear zone in the Tasiast area. Besides, a total of 55 samples were collected from the two boreholes (TA15049DD and TA17070DD) situated in the West Branch and Piment sectors, respectively (Figure 4). The sampling was guided by variations in lithology and visible mineralization.

Moreover, a series of analytical techniques were employed, including optical microscopy (using a DM750 type microscope, Leica®), scanning electron microscopy (SEM) (using the Jeol JSM-7500 F type), and cathodoluminescence (CL) employing the cold-cathode method with a defocused beam (with 15 kV for electron acceleration voltage and 500 μA for current). The mineralogical composition of the bulk rock was then identified using an X-ray powder diffraction (XRPD) conducted with a Philips PW 1820 diffractometer and CuKα radiation (40 kV, 30 mA), and the diffraction data were analyzed via X'Pert High Score Plus software. Mineral quantification is based on the calculation of the integrated peak area of respective mineral phases multiplied by published weight factors (López-Galindo et al., 1996). Therefore, this study follows a comparative approach between mineralogical and petrographic studies of two representative boreholes from two selected areas in the Tasiast deposit.

RESULTS

Petrographic analysis

In this study, most of the rocks have a sedimentary nature, including greywacke, siltstone and banded iron formation, which primarily consists of a clastic sedimentary sequence dominated by quartzite and intruded by felsite dykes. The sedimentary unit has undergone significant shearing and retains a distinct phyllosilicate foliation. However, greywacke and siltstone primarily originated from the weathering of the volcanoclastic rocks, which mainly formed a turbiditic-clastic unit. However, in the following, a detailed synthesis of petrographic and mineralogical descriptions of mineral phases and the polyphase characteristics of the crossed levels is provided.

Banded Iron Formation (BIF)

Banded Iron Formation was identified in both boreholes at various depths, with thicknesses more prominent in the Piment than in the West Branch sector. The BIF is typically black, with alternating light and dark beds. The layers are generally, from millimeters to centimeters thick. According to the microscopic observations, the BIF mainly consists of alternating layers of quartz and magnetite. In some layers, biotite and garnet are also present and represent original pelitic layers; the dark layers consist of biotite, opaque minerals, and deformed amphiboles (hornblende or cummingtonite). Large garnets with a very skeletal and fractured appearance are connected to amphiboles by inclusions of quartz (Figure 5 A-D).Orientated and distorted biotite, garnets with quartz inclusions and bleached carbonates give the rock a crystalline appearance reminiscent of metamorphic rocks.

The presence of pyrite crystals around some sulfides in the blades was confirmed by X-ray diffraction (XRD) and scanning electron microscopy (SEM), which revealed pyrrhotite associated with gold (Figure 7). Pyrite is more

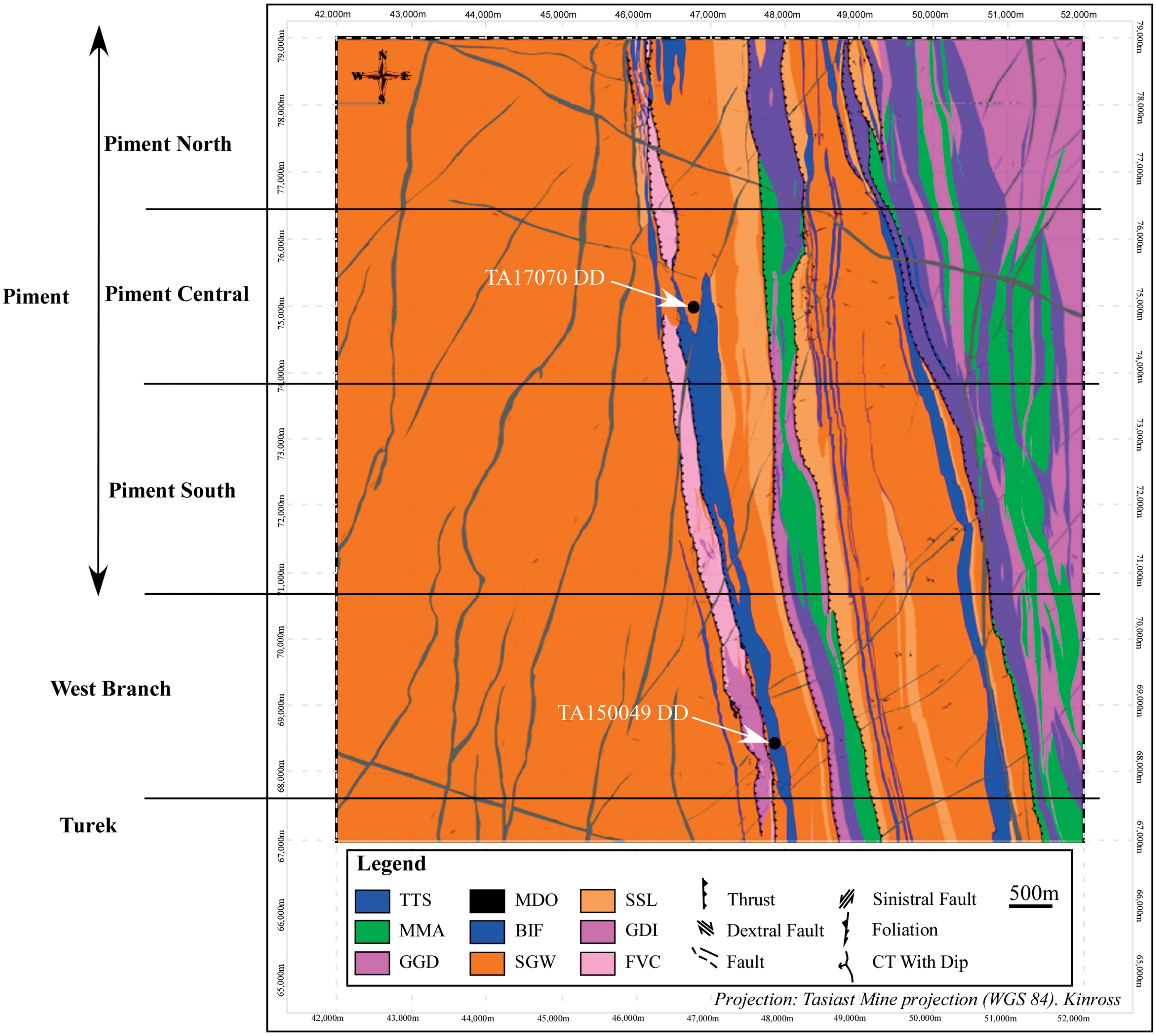

Figure 3. The geological map of El-Gaicha showing the selected boreholes within black circles and the different lithological units in West Branch and Piment (Isselmou Eghlmbitt et al., 2018; modified).

widespread in the BIF than is pyrrhotite, in contrast to the BIF in the West Branch.

Siltstone (SVC)

Siltstone is metasedimentary rock made up primarily of silt and clay minerals. Compared with the West Branch borehole, the Piment borehole displays only two levels with depths of less than 60 m. These rocks exhibit a fine- to intermediate-grained texture, with sandstone beds distinguished by their color. Under the microscope, plagioclase grains are frequently altered, and the abundance of muscovite is greater than that of other rocks in the area. Both boreholes contain simple twin orthoclase and microcline feldspars. However, Figure 5 E,F shows an example of calcite veins that displayed important alterations between the quartz and feldspar crystals from the transparent layers of this rock series, which clearly shows deformation in this area. Finelly, the siltstone has layers rich in muscovite, biotite and the main accessory mineral present is tourmaline, which is more abundant within three zones in the Piment borehole.

Felsite (FVC)

The felsite dykes levels in the lithological records of

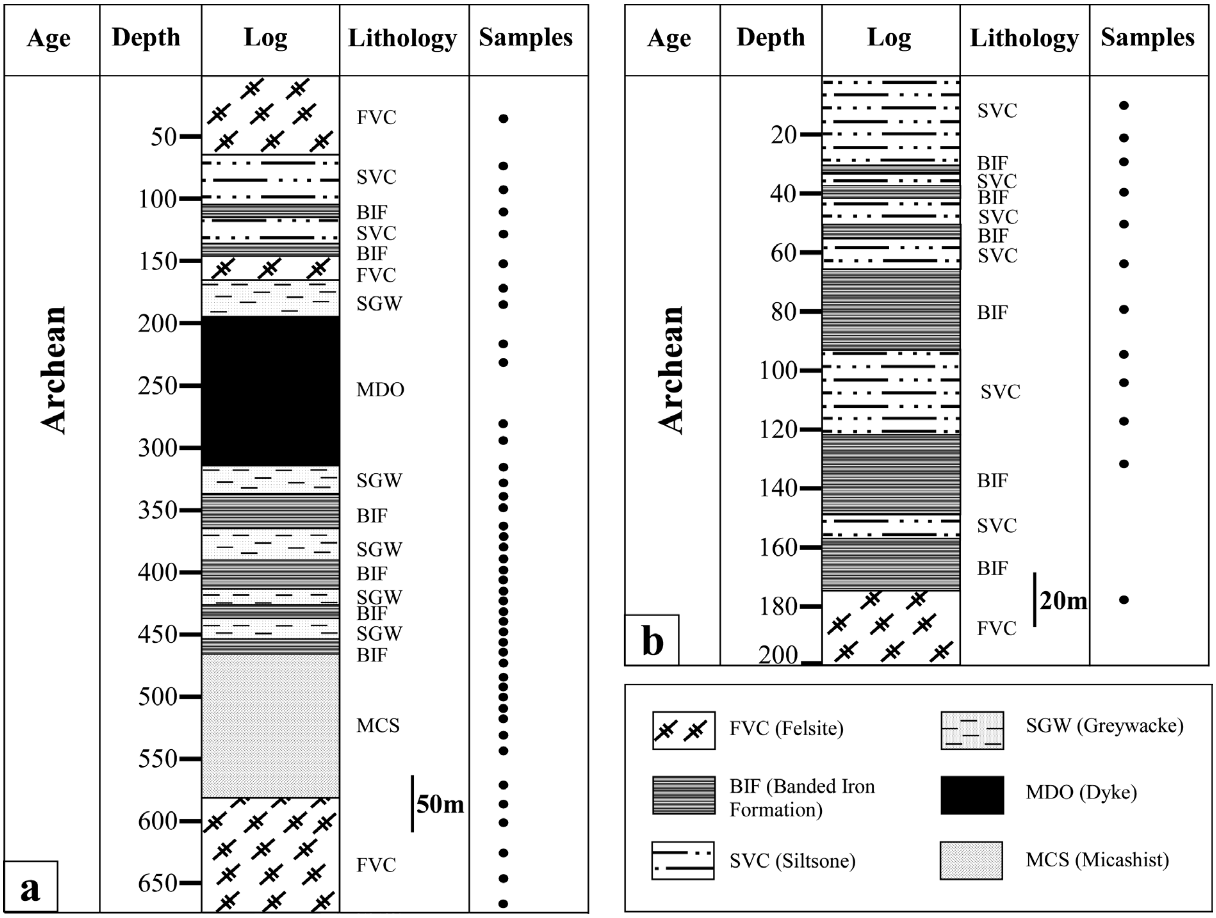

Figure 4. Lithological logs description of TA15049DD (a) and TA17070DD (b) boreholes.

Piment and West Branch significantly differ in depth and thickness (Figure 4). From top to bottom, the lithological log (TA15049DD) in the West Branch has three layers, whereas TA17077DD has only one level of felsite in the Piment area. The felsite at the macroscopic scale shows alternating light and dark gray bedding, with some intervals containing well-preserved quartz and/or feldspar phenocrysts. Furthermore, microveins composed of quartz and carbonates are present within the felsite dyke. Microscopic observations revealed an aplitic texture composed of minerals, e.g., quartz and feldspar crystals (Figure 6 A,B). The lepidoblastic structure at certain intervals is characterized by micas arranged in lamellae and clear cleavage blades. In addition, the blades contained feldspars, including plagioclase deformed amphiboles, hexagonal tourmalines with blue cores, and zoned muscovite. Opaque minerals are also present. The alteration was originally believed to be albite and commonly overlies biotite alteration in the FVC. Muscovite is linked with carbonates, which appear as veins in two distinct phases, each with different luminescent colors, yellow and orange.

Mica-schist (MCS)

The two lithological logs show a single level of mica schist in the Piment target at a depth of 470 m (Figure 4). The absence of mica-schist in the West Branch drilling can be attributed to the fact that it did not reach a depth of 200 m. When examining this rock under a microscope, it is possible to observe that mica-schist is arranged in broad lamellae and is visually emphasized by white mica scintillations. The foliaceous structure, which is predominantly composed of quartz and mica, is clearly discernible, and the mica-schist exhibits a schistosity structure with aligned phyllites containing muscovite, green chlorite and zoïsites with hornblende (Figure 6 C,D). The light color rock of the core is composed of quartz and feldspars, and the two types of amphiboles are dark, green and blue, with tourmaline inclusions in the garnets. These mica-schists samples have alternating

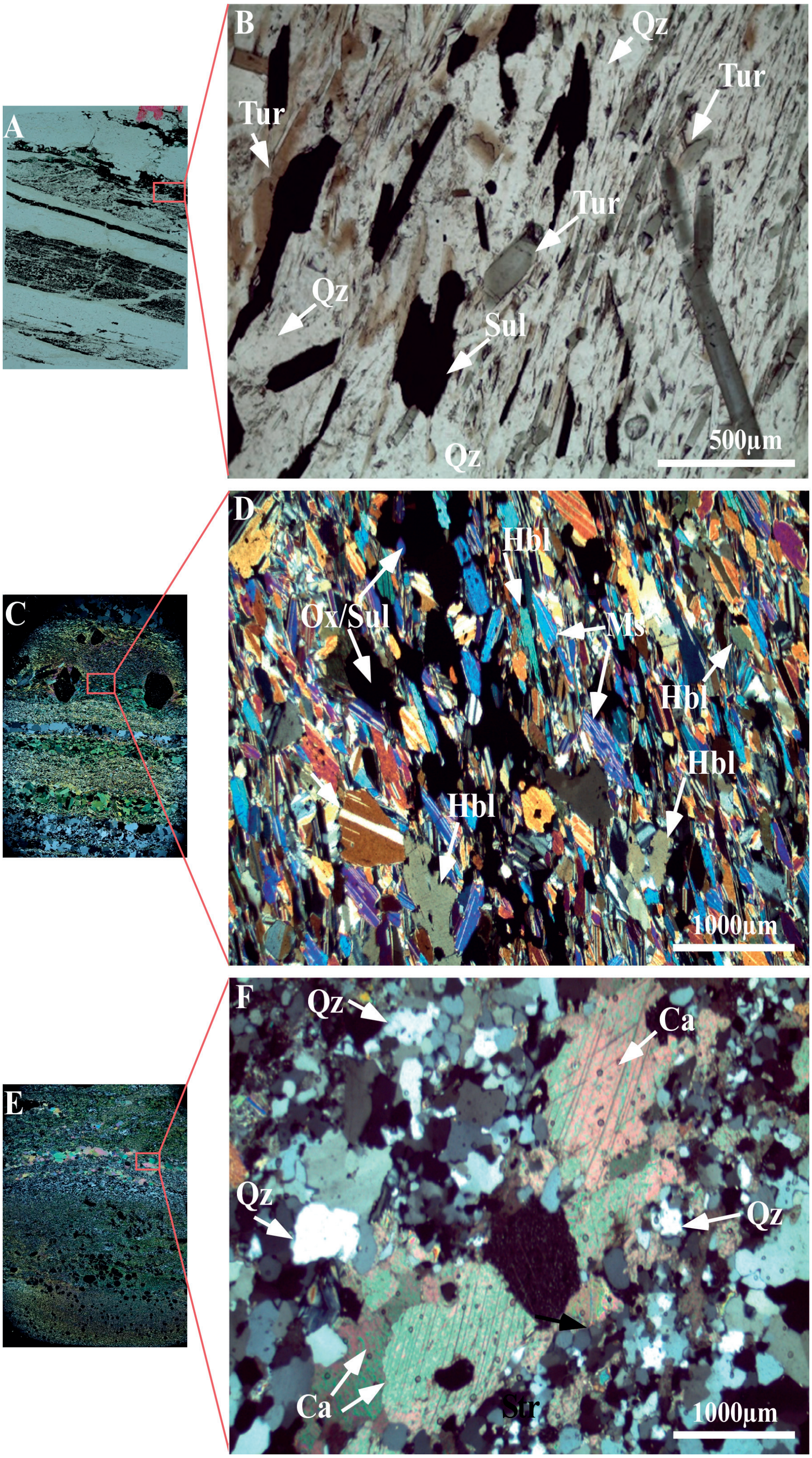

Figure 5. Photomicrographs of the BIF in Piment samples with: A: Scanned thin section, B: photomicrographs showing: tourmaline (Tur), quartz (Qz) and sulfide (Sul). C-D: photomicrographs of the BIF in West Branch showing: Oxide (Ox), sulfide (Sul), Muscovite (Ms) and Hornblende (Hbl). E-F photomicrographs of the SVC in West Branch (sample) showing: quartz (Qz) and calcite (Ca).

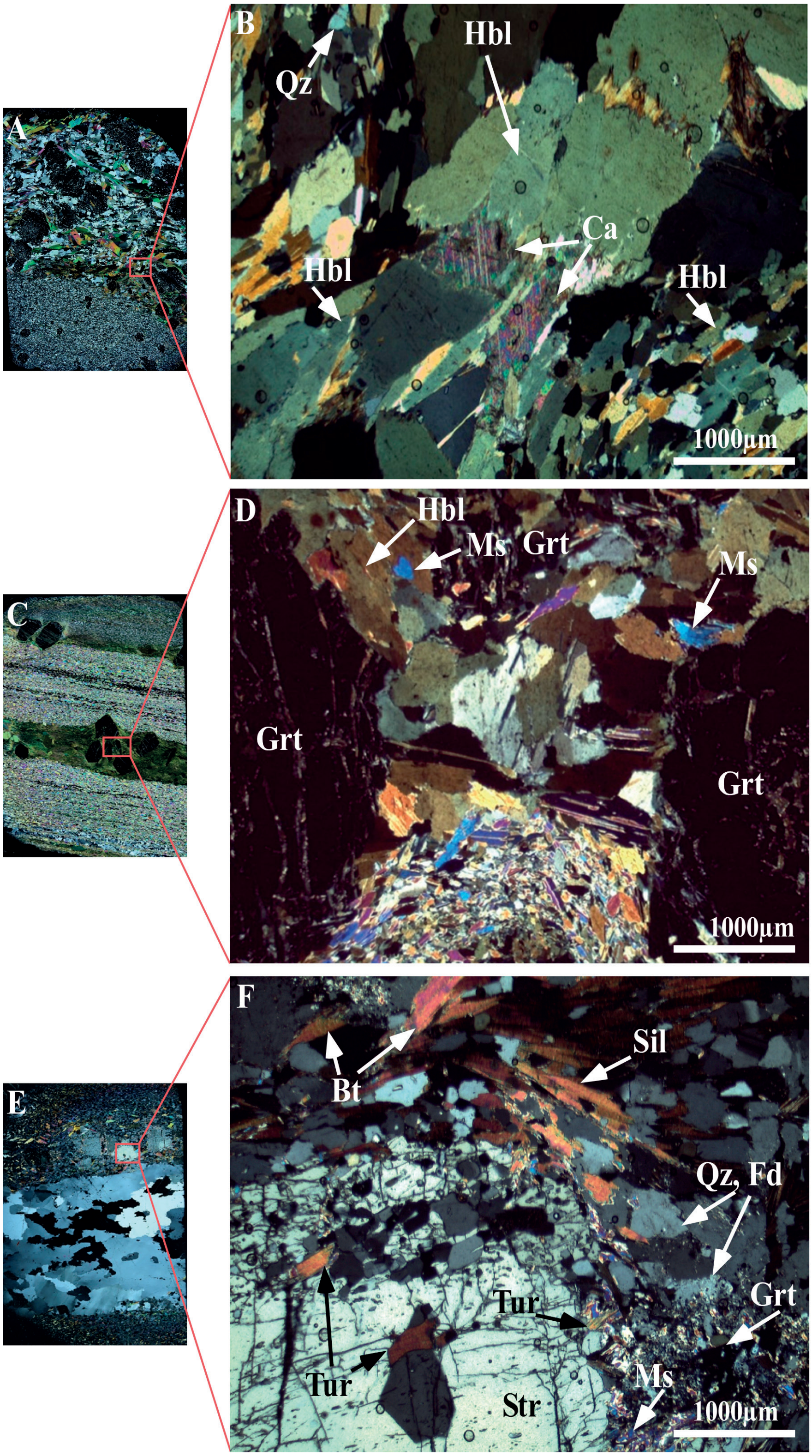

Figure 6. Photomicrographs from in the FVC of Piment sample, with: A: Scanned thin section, B: photomicrographs showing: quartz (Qz), calcite (Ca) and hornblende (Hbl). C-D: Photomicrographs in the Mica-schist of West Branch showing: hornblende (Hbl), muscovite (Ms) and garnet (Grt). E-F: Photomicrographs of SGW in the West Branch showing: biotite (Bt), quartz (Qz), feldspar (Fd), tourmaline (Tur), garnet (Grt), staurolite (Str) and sillimanite (Sil).

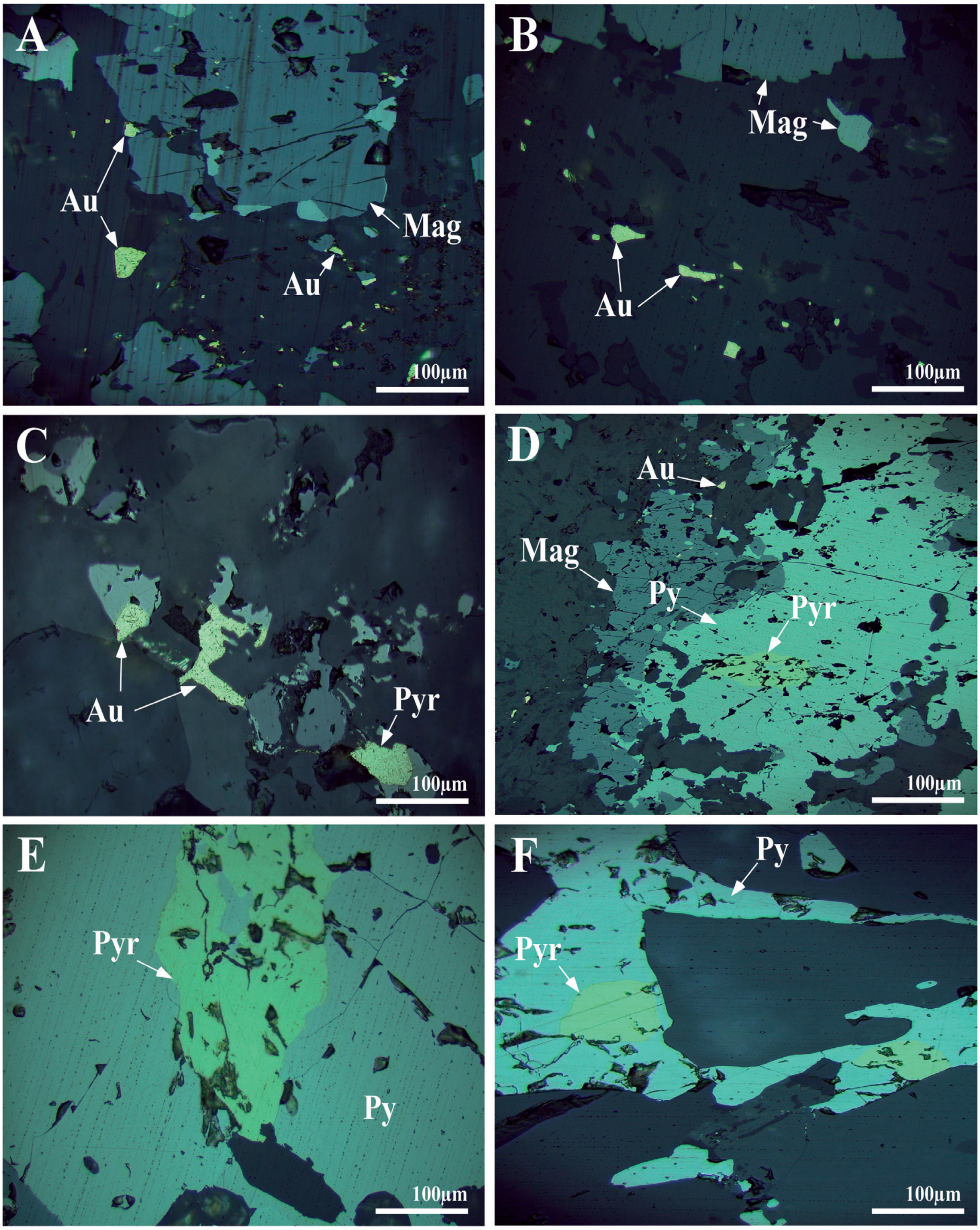

Figure 7. Photomicrographs of polished sections in reflected light showing gold grains in the SGW of West Branch (A-B) and in BIF of Piment (C-D and E-F) showing: pyrite (Py), pyrrhotite (Pyr), Magnetite (Mag) and gold (Au).

laminations rich in quartz, carbonate, and chlorite as well as biotite-rich laminations. In addition, sulfide minerals such as pyrite, pyrrhotite and even arsenopyrite are included in carbonate and biotite.

Greywacke (SGW)

The greywacke is a green rock that formed from volcanic activity and sedimentation. It has a distinct foliation pattern due to the alternating layers of dark, biotite-rich sections and darker, greenish areas with chlorite. In the West Branch log, only four layers of SGW are present, intermixed with BIF and intersected by a dyke. Garnet grains are visible in the SGW, appearing as reddish particles ranging in size from 2 to 7 mm. Microscopic observations reveal that the rock is composed of grains of quartz, plagioclase and mica lamellae. Moreover, muscovite is present in significant quantities, and biotite is prominent in highlighting the foliation. The presence of tourmaline has the potential to reflect the environment in which they formed, as they are extremely rich in tourmaline, zoïsites emanate from calcium plagioclase hydrothermal alteration (Figure 6 E,F). Additionally, the presence of chlorites, which exhibit a greenish color and blue tint characteristic of secondary biotite, was noted (Uytenbogaardt and Burke, 1985). Quartz veinlets intersected by earlier tourmalines, and garnets crunched with inclusions of biotite and tourmaline were also observed. Furthermore, other minerals, including centimeter-sized fibrotic tufts of sillimanite, were detected. These tufts, which are very common at this level, are formed by secondary biotite and can also be formed by metamorphism.

The greywacke rock shows mineralized zones with gold particles, which are associated with crystals of pyrite, pyrrhotite, arsenopyrite-and magnetite (Figure 7). These minerals were identified via reflected light and confirmed by SEM (Figure 8). Mineralization primarily occurs in thin veins that run parallel to the rock's foliation, and their sizes vary from millimeters to centimeters. Moreover, the presence of these secondary minerals, which affect feldspar crystals, such as plagioclase, which transforms into calcite, suggests various alteration stages associated with gold mineralization. In addition, calcite and twinned apatite were identified by their reflectivity via cathodoluminescence (Figure 9), and some minerals experienced visible hydrothermal alteration, which further suggested the presence of an active hydrothermal system in the study area.

In addition, the metamorphic assemblage contains widely distributed biotite. However, in the mineralized zone, the emergence of a second generation of biotite of hydrothermal origin, which is accompanied by strong matrix solidification in this greywacke facies, was observed. Given that biotite is smaller (30 to 50 µm versus 100 to 300 µm) and has greenish brown instead of reddish brown pleochroism. However, hydrothermal biotite can be distinguished from metamorphic biotite.

Dykes

Doleritic and gabbroic dykes are formed late in geological succession and differ from mineralization. However, the system is complicated. These dykes normally consist of basaltic material but could also be dolerite or gabbro due to the large thermal differential that exists between the gabbroic dykes and their surroundings, and their borders are typically doleritic.

Mineralogical analysis

To confirm the microscopic observations, the mineralogical composition of the collected samples was determined via X-ray diffractometry. The diffractometric analysis allowed us to establish a mineral paragenesis of the levels crossed by the two drillings (Figure 10).

The distributions of the various mineral phases encountered in the borehole samples as a function of depth are presented in Tables 1 and 2. The major mineral constituents are quartz, feldspar, biotite, muscovite, amphibole (hornblende), garnet, chlorite, and the less abundant minerals are magnetite, hematite and cummingtonite. However, other minerals, such as gold, carbonates (calcite), sulfides (pyrite, pyrrhotite, and arsenopyrite), tourmaline, actinolite, zoisite and fuchsite, were later intruded by alteration processes (Figure 11). On the other hand, the primary minerals are quartz, feldspar, and biotite, while the hydrothermal minerals are basically tourmaline, muscovite, calcite, amphibole, gold, pyrite and pyrrhotite.

DISCUSSION

The gold mineralization in the Tasiast deposit is essentially related to the hydrothermal system. It begins with the formation of biotite and feldspar, which are associated firstly with quartz, calcite and apatite, that are overprinted by the main gold mineralization, and secondarily with tourmaline, pyrite and pyrrhotite.

The abundance of some elements, such as Fe-silicates in the veins, varies widely, partially reflecting the nature of the host rocks but also possibly through the evolution of the composition of the fluid phase via wall–rock interactions. Indeed, the veins contain variable amounts of other minerals, including garnet, magnetite, muscovite, carbonate, quartz, and hornblende, accompanied by variable amounts of chlorite, cummingtonite, pyrrhotite and pyrite. In addition, carbonate veins and associated alteration constitute the last significant hydrothermal stage recognized. However, the lithostratigraphic context of Tasiast is dominated by alternating metavolcano-sedimentary rocks, which are approximately 2.8 Ga in age (Chardon, 1997; Key et al., 2008; Heron et al., 2016; Bhuiyan et al., 2022). The sequence consists of meta-greywacke, siltstones, magnetic banded iron formation, felsite and mica- schist; this sequence is intersected by doleritic to gabbroic dykes.

Petrographic observations, as well as mineralogical analyses, confirm that mineralization is related to sulfides that typically appear contemporaneous with biotite and

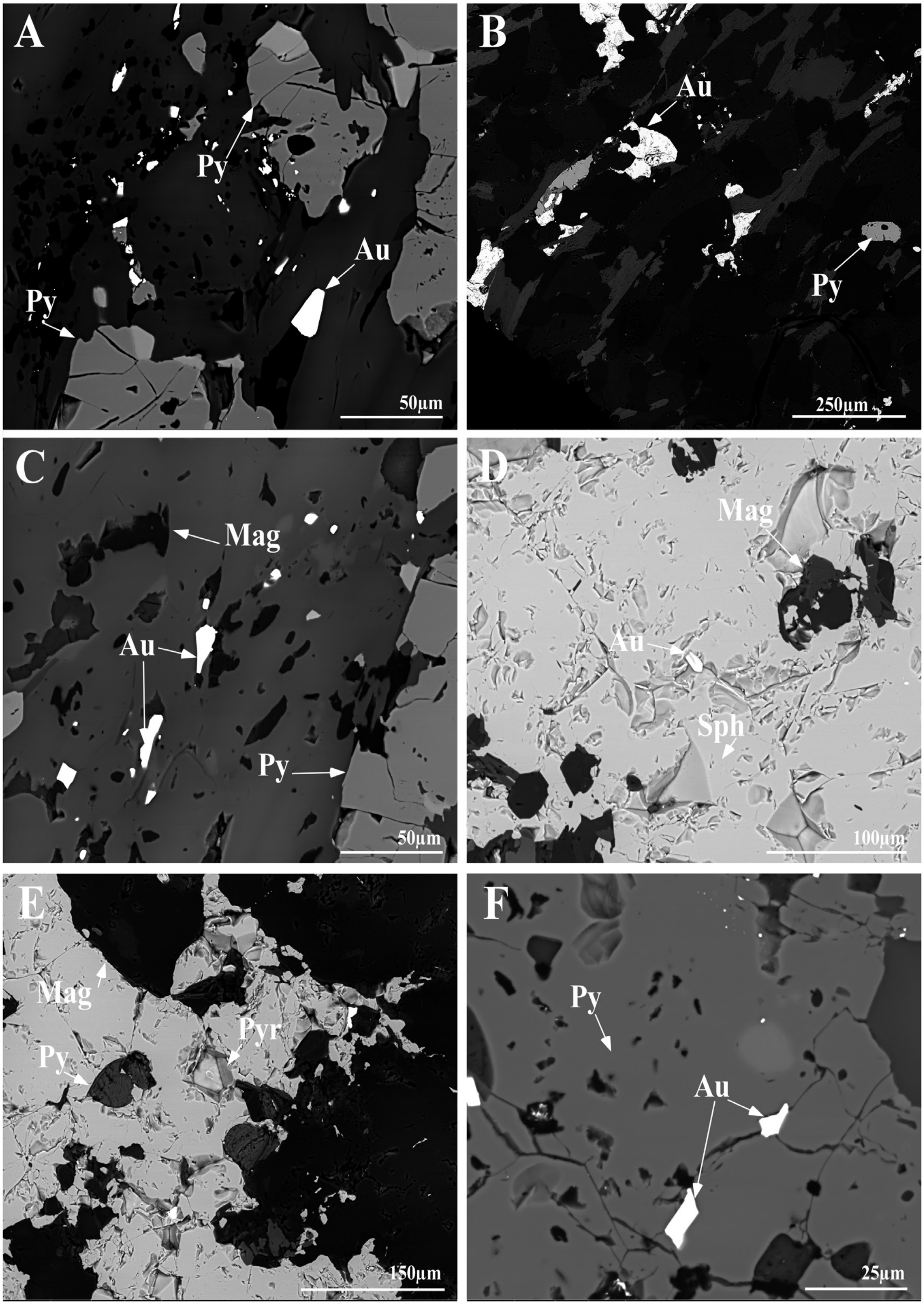

Figure 8. SEM images photomicrographs showing: (A, B) pyrite (Py) intergrowth with native gold (Au) in quartz vein and gangue minerals; (C, D): Pyrite and magnetite (Mag) with micro inclusions of native gold in sphalerite (Sap); (E, F): Two phase's inclusions of native gold and pyrrhotite (Pyr) with magnetite imbedded in gangue minerals.

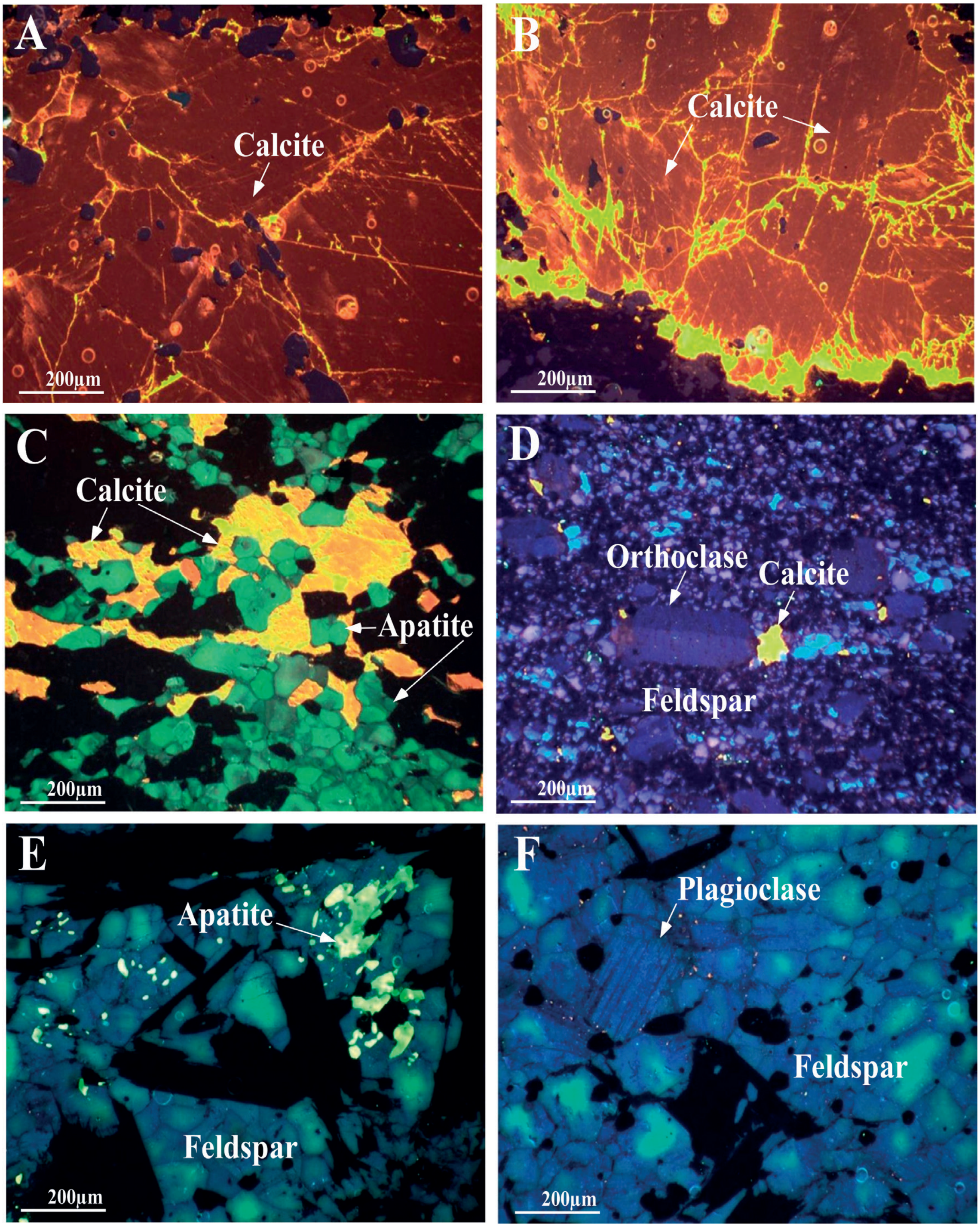

Figure 9. Cathodoluminescence microscopy photomicrographs showing: (A, B): Calcite vein with an intense orange luminescence; (C): Apatite prevails a green luminescence with inclusion of over-orange luminescence calcite; (D): feldspar (a mineral with blue luminesces) with orthoclase prevails (dark grey in black and white) related to the inclusion of calcite with a prevails yellowish luminescence; (E): Apatite and feldspar with green luminescence; (F): Polysynthetic plagioclase with light blue and green luminescence, the difference in coloration of feldspar (with blue and others with green luminescence) indicates that are from different generations and being evident that the blue feldspars are later than the green one.

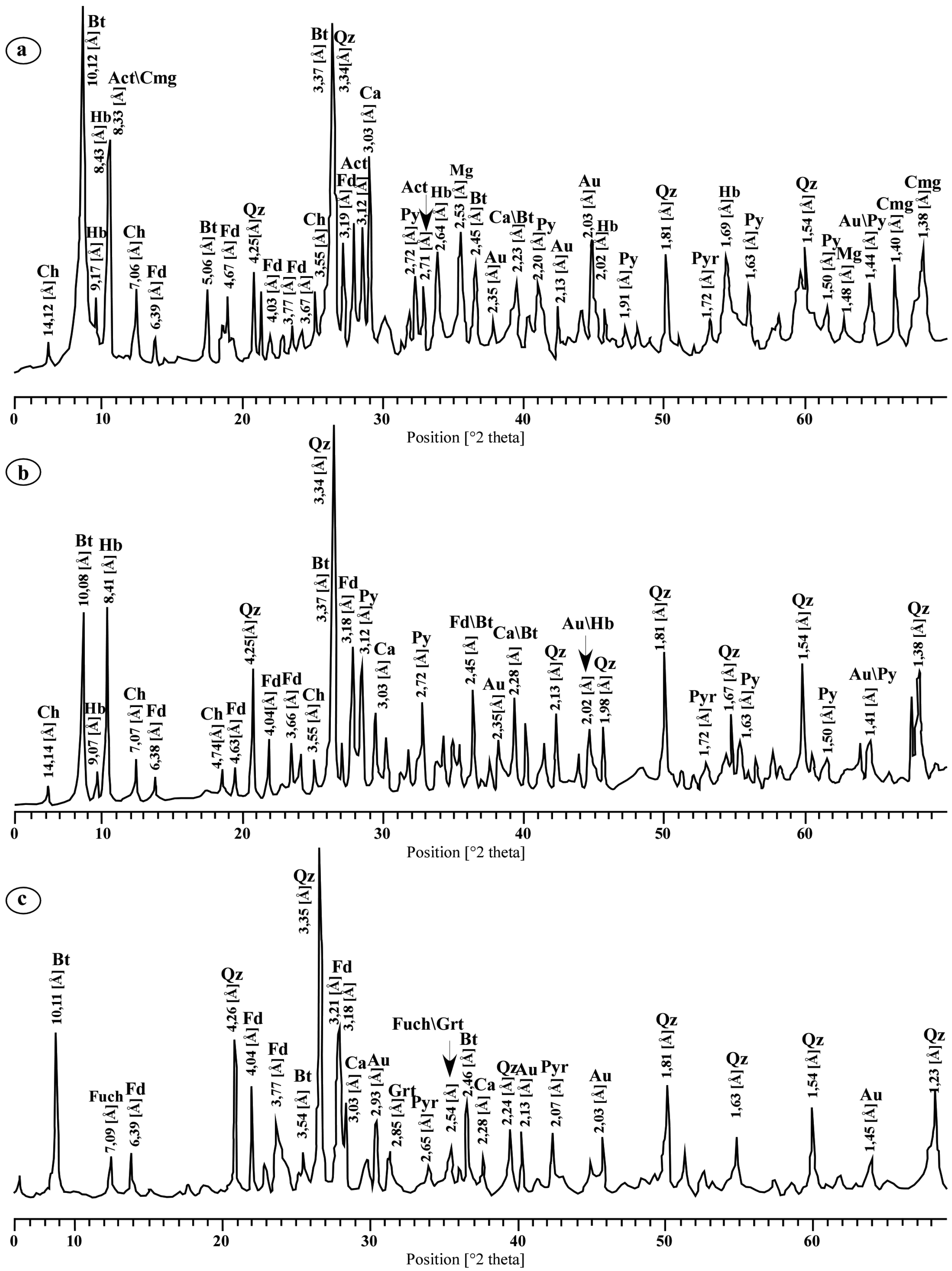

Figure 10. X-ray powder diffraction patterns of total rock of samples from the: a) BIF of TA17077DD borehole, b) Greywacke of TA15049DD borehole, and c) Felsite from TA15049DD borehole. With: Qz: quartz; Fd: feldspar; Ca: calcite; Bt: biotite; Ch: chlorite; Grt: garnet; Hb: hornblende; Mag: magnetite; Py: pyrite; Pyr: pyrrhotite; Act: actinolite; Cum: cummingtonite; Fuch: fuchsite; Au: gold.

Table 1. Mineralogical composition of the bulk samples of the TA150049DD borehole. (% weight/weight).

Samples	Depth (m)	Rock type	Whole-rock mineralogy																		
			Qz	Fd	Ca	Bt	Ms	Ch	Grt	Hbl	Mag	Hem	Gold	Py	Arsp	Pyr	Tur	Act	Cum	Zoit	Fuch
1	33,8	Felsite	25	15	7	10	18	8	-	5	-	-	-	-	-	-	2	-	-	5	5
2	91	Siltstone	35	20	3	15	-	4	4	10	5	2	-	2	-	-	-	-	-	-	-
3	101,1	Siltstone	32	18	5	10	10	-	5	10	-	-	-	2	-	1	5	-	-	2	-
4	128,15	Siltstone	26	15	2	15	20	5	8	-	-	-	-	-	-	5	2		2	-	-
5	140,2	BIF	40	15	2	11	-	-	4	4	10	5	-	7	-	-	-	2	-	-	-
6	145,9	BIF	35	15	-	13	-	-	5	15	7	5	-	5	-	-	-	-	-	-	-
7	162	Greywacke	20	12	10	15	10	-	7	2	-	-	3	5	3	6	5	-	-	2	-
8	184,9	Dyke	30	20	-	8	-	5	-	26	-	-	-	-	-	-	5	4	2	-	-
9	198	Dyke	25	17	6	12	8	-	-	15	-	-	-	2	3	-	5	-	3	4	-
10	213,6	Dyke	23	13	12	20	2	-	10	-	-	-	-	-	-	3	12	-	-	5	-
11	237,35	Dyke	35	15	-	12	-	-	7	15	-	-	-	15	-	-	-	1	-	-	-
12	245,1	Dyke	25	12	-	15	20	-	-	17	-	-	-	6	-	-	5	-	-	-	-
13	257,9	Dyke	30	15	-	8	15	4	5	11	-	-	-	1	-	-	3	2	6	-	-
14	268,3	Dyke	25	15	-	8	17	5	5	16	-	-	-	-	-	-	-	3	6	-	-
15	274,9	Dyke	28	25	-	10	8	3	-	18	-	-	-	-	-	-	-	3	5	-	-
16	280,9	Dyke	30	20	-	8	-	5	-	26	-	-	-	-	-	-	5	4	2	-	-
17	284,6	Dyke	25	17	6	12	8	-	-	15	-	-	-	2	3	-	5	-	3	4	-
18	301,55	Dyke	23	19	12	14	2	-	10	-	-	-	-	-	-	3	12	-	-	5	-
19	306,1	Dyke	32	15	6	10	7	-	-	11	-	-	-	2	3	-	5	-	3	6	-
20	316,95	Dyke	33	20	-	12	9	2	2	18	-	-	-	1	-	-	-	1	2	-	-
21	328,25	BIF	28	12	3	10	8	-	5	7	5	3	1	5	-	-	1	7	5	-	-
22	350,55	BIF	30	15	5	8	5	-	6	5	9	2	1	3	-	-	2	5	4	-	-
23	365,35	BIF	26	12	4	6	5	2	5	7	10	3	-	5	-	3	3	4	5	-	-
24	368,55	Greywacke	26	15	4	7	5	4	5	7	-	-	7	7	-	3	5	-	5	-	-
25	376,15	BIF	30	12	1	10	8	-	5	7	5	3	1	5	-	-	1	7	5	-	-
26	382,15	BIF	28	15	7	8	5	-	6	5	7	2	1	5	-	-	2	5	4	-	-
27	387,3	BIF	25	15	1	7	6	8	2	3	10	8	2	2	-	2	-	4	5	-	-
28	396,15	BIF	28	17	-	10	5	6	3	7	7	5	2	1	-	-	-	3	6	-	-
29	420,7	Greywacke	27	14	5	10	7	3	5	10	-	-	5	3	-	9	1	-	-	1	-
30	425	BIF	33	15	4	8	5	-	6	5	9	2	1	2	-	-	2	4	4	-	-
31	432	Greywacke	32	15	4	7	5	4	5	9	-	-	2	3	-	6	5	-	3	-	-
32	451	Micashist	18	10	8	20	12	10	3	5	-	-	-	2	1	3	2	-	-	6	-
33	462,5	Micashist	18	12	7	12	15	8	5	12	-	-	-	3	1	2	2	-	-	3	-
34	473,9	Micashist	19	14	-	13	17	4	4	16	-	-	-	3	-	2	3	1	2	2	-
35	489,3	Micashist	18	15	3	10	17	5	6	8	-	-	-	4	-	5	5	-	2	2	-
36	502	Micashist	18	13	3	15	16	9	5	8	-	-	-	-	-	2	4	-	4	3	-
37	522,8	Micashist	19	17	-	12	13	10	6	9	-	-	-	-	-	3	2	2	3	4	-
38	547,9	Micashist	19	12	-	10	16	10	8	11	-	-	-	3	-	5	2	-	2	2	-
39	587,15	Felsite	27	12	7	15	12	8	-	5	-	-	-	-	-	-	2	-	-	7	5
40	593,85	Felsite	25	15	9	10	11	6	-	7	-	-	-	-	-	-	5	-	-	6	6
41	596	Felsite	28	10	6	11	10	5	-	9	-	-	-	4	-	5	-	-	-	5	7
42	600,45	Felsite	29	13	8	15	7	9	-	3	-	-	-	-	-	-	5	-	-	7	4
43	611,1	Felsite	28	12	7	14	15	6	-	10	-	-	-	-	-	-	2	-	-	6	-

With: BIF: Banded Iron Formation; Qz: Quartz ;Fd: Feldspar; Ca: Calcite; Bt: Biotite; Ms: Muscovite; Ch: Chlorite; Grt: Garnet; Hbl: Hornblende; Mag: Magnetite; Hem: Hematite; Py: Pyrite; Arsp: Arsenopyrite; Pyr: Pyrrhotite; Tur: Tourmaline; Act: Actinolite; Cum: Cummingtonite; Zoit: Zoisite; Fuch: Fuchsite.

Table 2. Mineralogical composition of the bulk samples of the TA17070DD borehole. (% weight/weight).

Samples	Depth (m)	Rock type	Whole rock mineralogy																		
			Qz	Fd	Ca	Bt	Ms	Ch	Grt	Hbl	Mag	Hem	Gold	Py	Arsp	Pyr	Tur	Act	Cum	Zoit	Fuch
1	23,7	Siltstone	25	15	2	25	18	13	-	-	-	-	-	2	-	-	-	-	-	-	-
2	30,5	Siltstone	28	20	5	18	10	9	-	2	-	-	-	1	-	-	-	2	5	-	-
3	38,4	BIF	32	15	-	10	-	-	5	8	12	2	3	10	-	-	3	-	-	-	-
4	45,1	Siltstone	26	15	5	15	20	2	7	-	-	-	-	1	-	4	2	3	-	-	-
5	47,4	BIF	35	10	-	10	4	-	4	7	10	5	3	7	-	-	-	-	5	-	-
6	62,8	BIF	40	10	8	13	-	-	5	8	-	2	4	5	-	-	-	5	-	-	-
7	90,8	Siltstone	27	12	8	10	10	4	7	-	-	-	-	5	3	5	5	2	-	2	-
8	103,4	BIF	30	10	10	8	-	-	7	5	12	5	5	4	-	-	-	4	-	-	-
9	113,3	BIF	25	17	2	12	8	-	8	5	-	-	2	2	3	-	5	2	2	7	-
10	125,1	BIF	28	13	10	20	2	-	5	-	-	-	2	4	-	3	3	5	-	5	-
11	142,5	BIF	35	15	6	12	5	-	7	7	-	5	3	2	-	-	-	3	-	-	-
12	174,15	Felsite	25	12	-	15	20	4	-	8	-	-	-	2	-	-	5	2	-	-	7

With: BIF: Banded Iron Formation; Qz: Quartz ;Fd: Feldspar; Ca: Calcite; Bt: Biotite; Ms: Muscovite; Ch: Chlorite; Grt: Garnet; Hbl: Hornblende; Mag: Magnetite; Hem: Hematite; Py: Pyrite; Arsp: Arsenopyrite; Pyr: Pyrrhotite; Tur: Tourmaline; Act: Actinolite; Cum: Cummingtonite; Zoit: Zoisite; Fuch: Fuchsite.

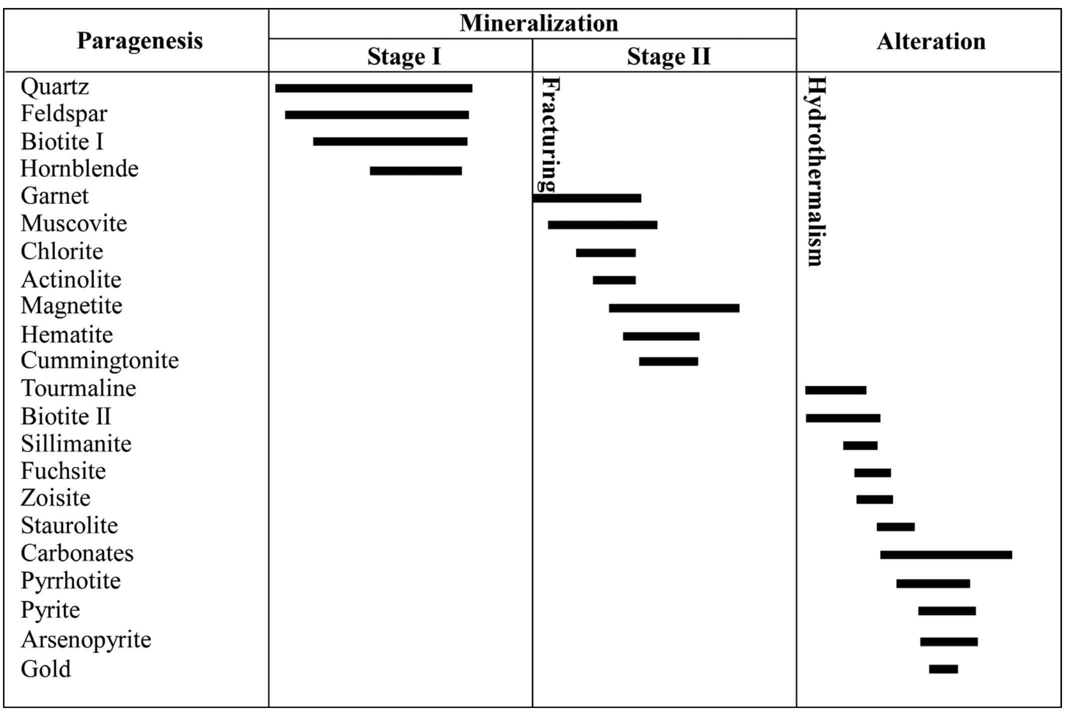

Figure 11. Paragenetic sequence diagram of mineral assemblages from Tasiast deposit. The lengths of lines indicate relative abundances of minerals.

amphibolite. Fe silicates, quartz are associated mainly with pyrrhotite, pyrite, and in some cases, with minor sphalerite and arsenopyrite. Throughout the Piment deposit, gold is associated with silica flooding and magnetite sulfidation (Figure 8). The mineralization in the BIF and the biotite-amphibole-tourmaline stage are likely components of the same mineralization event because of their striking mineralogical similarities (Pollard, 2012).

As seen in greywacke and banded iron formation units, gold is connected to silicification and to the substitution of sulfides and magnetite.

The altered mineral assemblage is associated mainly with brittle–ductile thrusts branching from the Tasiast Thrust. The occurrence of gold is related to pyrite, pyrrhotite, magnetite and sphalerite (Figures 7 and 8) and is typically found in zones of mineralization that are associated with faults and shear zones. Eglinger et al., 2023 suggested that this mineralization is likely related to deformation events that occurred at the regional scale. The age of 2839±36 Ma obtained by hydrothermal overgrowth on zircons from a quartz vein is interpreted as representing the age of mineralization at Tasiast (Heron et al., 2016).

At West Branch, gold occurs in quartz–carbonate veins that are folded and locally transposed parallel to the main foliation, which is axial and flat to the folds. The hydrothermal system is responsible for the gold mineralization determined by the inductively altered minerals of the hydrothermal alteration and the neoformed minerals of the metamorphism.

Additionally, the appearance of apatite in the CL observations (Figure 9) is more likely to have a hydrothermal origin (Gromet and Silver, 1983; Belousova et al., 2002; O'Sullivan et al., 2020).There is an abundance of quartz vein networks, and their relation to deformation likely indicates that mineralization was structurally controlled during hydrothermal events, which was linked to the circulation of fluids during the transpressive event. This phenomenon appears to have been active during the declining phases of brittle-ductile deformation after peak metamorphism. Moreover, deposits are commonly located in the third order of deformation (D_3), predominantly near large-scale compressional structures (Meriaud, 2020). The controlling structures are typically ductile to brittle and highly variable in type. The feldspar biotite, amphibole, tourmaline, pyrrhotite, sphalerite and gold veins are generally boudinized, whereas the zoïsite, muscovite, carbonate veins and late carbonate veins appear to be related to brittle fractures. Additionally, from the mineralogical point of view of each stage, the identification of staurolite as a metamorphic mineral marker of hydrothermal alteration during paragenesis indicates a decrease in temperature during the evolution of the system (Henry et al., 1985; Praveen et al., 2005; Taylor et al., 2007; Gaillard et al., 2018; Knorsch et al., 2020; Kouhestani et al., 2022).

Moreover, gold mineralization was associated with shear zones and formed during the approximate E–W shortening event that accompanied the inversion of the Tasiast sedimentary basin. This deformation gave rise to tight isoclinal, vertical to overturned folds, thrusts and trans-current shears throughout the Aouéouat belt (Markwitz et al., 2016b). Several sets of northeast- and northwest trending faults intersect the folds and locally offset the geological units (Heron et al., 2016). While orogenic gold deposits have consistent spatial and temporal compositions (Graves et al., 1998; Villeneuve, 2008), they were formed during deformational processes at convergent margins independently of the age of the host rock, which can include both Archean and Proterozoic greenstone belts. Furthermore, the present study shows that the Tasiast deposits were formed during this unique, transpressive tectonic event.

CONCLUSION

Mineralization in Tasiast district is strongly controlled by several lithological, hydrothermal and structural parameters. Indeed, lithological surveys have shown that gold mineralization is highly concentrated in the quartz-carbonate veins hosted in the specific shear zone and in some case controlled by the sulfide in banded iron formation (BIF) facies, which are both crossed by two drilling boreholes with considerable thickness and are marked by the presence of micro-quartz veins.

Mineralogical and petrographical investigations of the mining survey samples were conducted to understand the gold mineralization and associated sulfides in the West Branch and Piment sectors. In addition, the obtained results confirm that gold mineralization was controlled by strong hydrothermal alteration. The rock matrix has undergone significant hydrothermal activity, which is evident from the presence of minerals such as tourmaline, the partial or complete replacement of plagioclase with calcite, the biotite with chlorite, and the occurrence of staurolite, zoïsite and sillimanite.

The hydrothermal fluids carrying this mineralization are rich in Fe-silicates in veins, and the gold in the other facies is disseminated at the West Branch site. On the other hand, Piment mineralization is relatively related to BIF and is spatially associated with domains where relatively with high percentages of sulfide minerals (pyrite-pyrrhotite and arsenopyrite). The relatively iron-rich nature of the BIF may have promoted sulfidation and gold mineralization. The latter is spatially associated with the shear system of the Tasiast structure in the main shear zone as well as in the late veins.

The volcano-sedimentary stratigraphy has been tightly folded isoclinally and is cut longitudinally by shears that are subparallel to the predominant foliation. Additionally, gold mineralization formed in a sinistral transtensional tectonic regime. These shears are generally 5 to 10 m wide and exhibit strong bedding and mylonitic textures with distinct signs of hydrothermal alteration and quartz veining that developed along or parallel to these structures.

These shears favored the circulation of hydrothermal fluids and gold mineralization.

The banded iron formation (BIF) rocks are particularly important and host most high-grade gold mineralization. Therefore, the metamorphic rock sequence hosting this mineralization is characterized by intense foliation marked by the presence of micas and amphiboles. Additionally, gold is associated primarily with sulfides in quartz veins, so sulfidation is considered a crucial process in ore formation.

ACKNOWLEDGEMENTS

This study was financed by the Laboratory of Spectroscopic Characterization and Optical Materials (LaSCOM), University of Sfax, Faculty of Sciences. We express our thanks to the professors Siddig M Elzien, Sidi Mohamed Dahi, Moulay Mohamed and Osama Salah for their availability, recommendations and support during this work. We gratefully acknowledge Kinross Gold Corporation for providing us samples and geological data.

Conflict of interest declaration

The authors declare that they have no competing interests.

REFERENCES

Aïfa T., 2021. Mineralization and sustainable development in the West African Craton: from field observations to modelling. Geological Society of London, Special Publications, 502, 7 1-29.

Amadu C.C., Foli G., Kissi-Abrokwa B., Akpah S., 2021. Geostatistical Approach for The Estimation of Shear-Hosted Gold Deposit: A Case Study of The Obuasi Gold Deposit, Ghana. Malaysian Journal of Geosciences (MJG), 5(2), 76-84, doi: 10.26480/mjg.02.2021.76.84.

Barrère J., 1967. Le groupe précambrien de l'Amsaga entre Atar et Akjoujt (Mauritanie): étude d'un métamorphisme profond et de ses relations avec la migmatisation. Mémoires du BRGM, 42.

Bessoles B., 1977. Géologie de l'Afrique. Le craton ouest Africain. Mémoires de Bureau de Recherches Géologiques et Minières, 88. 402 pp.

Bhuiyan M., Esmaeili K., Ordonez-Calderon J.C., 2022. Evaluation of rock characterization tests as geometallurgical predictors of bond work index at the Tasiast Mine, Mauritania. Minerals Engineering 175, 107293, doi: 10.1016/j.mineng.2021.107293.

Blanchot A., 1955. Le Précambrien de Mauritanie occidentale (esquisse géologique). Thèse Nancy. Bulletin de la Direction fédérale des Mines et de la Géologie, Dakar, 17, 308 p.

Belousova E.A., Griffin W.L., O'Reilly S.Y., Fisher N.L., 2002. Igneous zircon: trace element composition as an indicator of source rock type. Contributions to mineralogy and petrology, 143, 602-622, doi: 10.1007/s00410-002-0364-7.

Boher M., Deschamps M., Rocci G., Abouchami W., Albarede F., Michard A., 1990. Lower Proterozoic crustal growth in Reguibat Rise (Mauritania): Geological and isotopic data. Publication occasionnelle-Centre international pour la formation et les échanges géologiques, 22, 75-78.

Bradley Dwight C., Holly Motts John D., Horton Stuart Giles A., Cliff Taylor D., 2015. Map of Mauritania compiled and prepared in cooperation with the Ministry of Petroleum, Energy, and Mines of the Islamic Republic of Mauritania. https://doi.org/10.3133/ofr20131280A1

Bronner G., 1992. Structure et Évolution d'un Craton Archéen: La Dorsale Réguibat Occidentale (Mauritanie) tectonique et métallogénie des formations ferrifères, 201. Éditions du BRGM, 448 p.

Chardon D., 1996. Les Déformations Continentales Archéennes: Exemples naturels et modélisation thermomécanique. Géologie appliquée. Thése de doctorat, Université Rennes I, 176p.

Dosso L., Vidal P., Sichler B., Bonifay A., 1979. Age précambrien de dolérites de la Dorsale Réguibat (Mauritanie). Comptes rendus Académie des sciences de Paris, 288, 739-742.

Eglinger A., André-Mayer A.S., Thébaud N., Masurel Q., 2023. West African Leo-Man Shield Metallogenic Province. Metallic Resources 2: Geodynamic Framework and Remarkable Examples in the World, 265-305.

El Abd Bouha M., Ouali H., Ouabid M., El Messbahi H., Mokhtari A., 2021. Petrogenesis and crustal evolution of the Tasiast TTG suite (SW Reguibat Shield, Mauritania). Implication for crustal growth in the West African craton. Comptes Rendus Géoscience, 353, 19-35, doi: 10.5802/crgeos.48.

Gaillard N., Williams-Jones A.E., Clark J.R., Lypaczewski P., Salvi S., Perrouty S... Linnen R.L., 2018. Mica composition as a vector to gold mineralization: Deciphering hydrothermal and metamorphic effects in the Malartic district, Quebec. Ore Geology Reviews 95, 789-820, doi: 10.1016/j.oregeorev.2018.02.009.

Groves D.I., Goldfarb R.J., Gebre-Mariam M., Hagemann S.G., Robert F., 1998. Orogenic gold deposits: a proposed classification in the context of their crustal distribution and relationship to other gold deposit types. Ore geology reviews, 13, 7-27, doi: 10.1016/S0169-1368(97)00012-7.

Groves D.I., Goldfarb R.J., Robert F., Hart C.J., 2003. Gold deposits in metamorphic belts: overview of current understanding, outstanding problems, future research, and exploration significance. Economic geology 98, 1-29, doi: 10.2113/gsecongeo.98.1.1.

Gromet L.P. and Silver L.T., 1983. Rare earth element distributions among minerals in a granodiorite and their petrogenetic implications. Geochimica et Cosmochimica Acta 2003, 47, 925-939, doi: 10.1016/0016-7037(83)90158-8.

Goldfarb R.J., André-Mayer A.S., Jowitt S.M., Mudd G.M., 2017. West Africa: The world's premier Paleoproterozoic gold province. Economic Geology 112, 123-143, doi: 10.2113/econgeo.112.1.123.

Hamoud A., El Hadi H., Tahiri A., Chakiri S., Mehdioui S., Baghdad B., ... Aoufa M., 2021. Mauritanian geological resources: A lever for sustainable regional development via geotourism. International Journal of Geoheritage and Parks 9, 415-429, doi: 10.1016/j.ijgeop.2021.11.003.

Haissen F., Cambeses A., Montero P., Bea F., Dilek Y., Mouttaqi A., 2017. The Archean kalsilite-nepheline syenites of the Awsard intrusive massif (Reguibat Shield, West African Craton, Morocco) and its relationship to the alkaline magmatism of Africa. Journal of African Earth Sciences, 127, 16-50, doi: 10.1016/j.jafrearsci.2016.08.019.

Hamimi Z., Chabou MC., Errami E., Fowler AR., Fello N., Masrouhi A., Leprêtre R., 2024. The Geology of North Africa. Springer Nature (Eds.), doi: 10.1007/978-3-031-48299-1.

Henry D.J. and Guidotti C.V., 1985. Tourmaline as a petrogenetic indicator mineral: an example from the staurolite-grade metapelites of NW Maine. American mineralogist, 70, 1-15.

Heron K., Jessell M., Benn K., Harris E., Crowley Q.G., 2016. The Tasiast deposit, Mauritania. Ore Geology Reviews 78, 564-572, doi: 10.1016/j.oregeorev.2015.08.020.

Higashihara M., Marutani M., Bellal A.O., Dioumassi B., Ousmane D., Emenetoullah L., 2004. Plate-tectonic and metallogenic evolutions of western Reguibat shield: proposition of a hypothesis. Prog. Abstr. Internat. Geol. Correlation Prog. Conf. 485 (UNESCO/IUGS), Nouakchott, 5-13 December, 10-13 pp.

Isselmou Eghlembit, Seyidna A.L., Valentine., 2018. Tasiast from West branch to Piment geological mapping, pp. 3-8.

Ishagh M.M., Pour A.B., Benali H., Idriss A.M., Reyoug S.A.S., Muslim A.M., Hossain M.S., 2021. Lithological and alteration mapping using Landsat 8 and ASTER satellite data in the Reguibat Shield (West African Craton), North of Mauritania: implications for uranium exploration. Arabian Journal of Geosciences 14, 2576, doi: 10.1007/s12517-021-08846-x.

Jiang J., Hu P., Zhang H., Cheng X., Wang J., Xiang W., 2022. Genetic types of gold deposits in Western Africa and their temporal and spatial distribution. Geological Bulletin of China, 41, 85-98, doi: 10.12097/j.issn.1671-2552.2022.01.007.

Key RM., Loughlin S.C., Gillespie M., Del Rio M., Horstwood M.S.A., Crowley Q.G., ... Hen-ney P.J., 2008. Two Mesoarchean terranes in the Rgueïbat shield of NW Mauritania. Geological Society London Special Publications, 297, 33-52, doi: 10.1144/SP297.3.

Knorsch M., Deditius A.P., Xia F., Pearce M.A., Uvarova Y., 2020. The impact of hydrothermal mineral replacement reactions on the formation and alteration of carbonate-hosted polymetallic sulfide deposits: A case study of the Artemis prospect, Queensland, Australia. Ore Geology Reviews 116, 103232.

Kouhestani H., Mokhtari M.A.A., Chang Z., 2022. Fluid inclusion and stable isotope constraints on the genesis of epithermal base-metal veins in the Armaqan Khaneh mining district, Tarom-Hashtjin metallogenic belt, NW Iran. Australian Journal of Earth Sciences 69, 844-860, doi: 10.1016/j.oregeorev.2019.103232.

Lahondère D., Thiéblemont D., Goujou J-C., Roger J., Moussine-Pouchkine A., 2003. Le Métour J., Cocherie A., Guerrot C., Notice explicative des cartes géologiques et gîtologiques à 1/200 000 et 1/500 000 du Nord de la Mauritanie, vol. 1. DMG, Ministère des Mines et de l'Industrie, Nouakchott.

López-Galindo A., Ruiz J.T., Lopez J.G., 1996. Mineral quantification in sepiolite-palygorskite deposits using X-ray diffraction and chemical data. Clay Minerals 31, 217-224, doi: 10.1180/claymin.1996.031.2.07.

Mahmoud H.O., Raji M., Adjour M., Vall I.B., 1996. Mineralization and Exploration Perspectives in the Oudiane Elkharoub Zone, Birimian Domain, Reguibat Shield, Mauritania. Open Journal of Geology, x 13(12), 1312-1330, doi: 10.4236/ojg.2023.1312057.

Manning C.E. and Ingebritsen S.E., 1999. Permeability of the continental crust: Implications of geothermal data and metamorphic systems. Reviews of Geophysics 37(1), 127-150, doi: 10.1029/1998RG900002.

Markwitz V., Hein K.A., Jessell M.W., Miller J., 2016a. Metallogenic portfolio of the West Africa craton. Ore geology reviews 78, 558-563, doi: 10.1016/j.oregeorev.2015.10.024.

Markwitz V., Hein K A., Miller J., 2016b. Compilation of West African mineral deposits: Spatial distribution and mineral endowment. Precambrian Research 274, 61-81, doi: 10.1016/j.precamres.2015.05.028.

Mignot E.L.E., Siebenaller L., Beziat D., Salvi S., Andre-Mayer A-S., Reisberg L., Velasquez G., Zimmernann C., Franceschi G., 2014. The Paleoproterozoic Copper- Gold deposit of Gaoua, Burkina Faso: evidence for a polyphased mineralization. Acta geologica Sinica, (English Edition) 88, 970-972.

Mikucki E.J. and Ridley J.R., 1993. The hydrothermal fluid of Archaean lode-gold deposits at different metamorphic grades: compositional constraints from ore and wallrock alteration assemblages. Mineralium Deposita 28, 469-481, doi: 10.1007/BF02431603.

Meriaud N., 2020. Litho-tectonic evolution and metallogeny of the Yaouré gold camp, Côte d'Ivoire West Africa; Integration into the southern West African craton evolution. Thesis of the degree of doctor of the university of Western Australia, 157 p., doi: 10.26182/wc5n-4123.

Montero P., Haissen F., El Archi A., Rjimati E., Bea F., 2014. Timing of Archean crust formation and cratonization in the Awsard-Tichla zone of the NW Reguibat Rise, West African Craton: A SHRIMP, Nd-Sr isotopes, and geochemical reconnaissance study. Precambrian Research 242, 112-137, doi: 10.1016/j.precamres.2013.12.013.

Moussa Hamath Ba., Jaffal M., Khalidou Lo., Youbi N., Dahmada M.E.M., Ibouh H., ... Söderlund U., 2020. Mapping mafic dyke swarms, structural features, and hydrothermal alteration zones in Atar, Ahmeyim and Chami areas (Reguibat Shield, Northern Mauritania) using high-resolution aeromagnetic and gamma-ray spectrometry data. Journal of African Earth Sciences 163, 103749, doi: 10.1016/j.jafrearsci.2019.103749.

Mykhailov V., Virshylo I., Zagnitko V., Kravchenko D., Dubyna O., Sukach V., 2023. A New Gold Ore District Tijirit in Mauritania (Western Sahara). In 17th International Conference Monitoring of Geological Processes and Ecological Condition of the Environment. (Vol. 2023, No. 1, pp. 1-5). European Association of Geoscientists & Engineers, doi: 10.3997/2214-4609.2023520231.

O'Sullivan G., Chew D., Kenny G., Henrichs I., Mulligan D., 2020. The trace element composition of apatite and its application to detrital provenance studies. Earth-Science Reviews 201, 103044, doi: 10.1016/j.earscirev.2019.103044.

Ouattara Z., Coulibaly Y., Boiron M C., 2021. Shear-hosted gold mineralization in the Oumé-Fettèkro greenstone belt, Côte d'Ivoire: the Bonikro deposit, doi: 10.1144/SP502-582 2019-103.

Phillips G.N., Groves D.I., Kerrich R., 1996. Factors in the formation of the giant Kalgocrlie gold deposit. Ore Geology Reviews 10, 295-317, doi: 10.1016/0169-1368(95)00028-3.

Pollard P.J., 2012. A Review of the Tasiast Mine, Mauritania, With Reference to the Regional Geology and Gold Mineralization. Society of Economic Geologists, Inc. Special Publication, 16, 145-159.

Potrel A., Peucat J.J., Fanning C.M., Auvray B., Burg J.P., Caruba C., 1996. 3.5 Ga old terranes in the West African Craton, Mauritania. Journal of the Geological Society 153, pp.507-510, doi: 10.1144/gsjgs.153.4.0507.

Potrel A., Peucat J.J., Fanning C.M., 1998. Archean crustal evolution of the West African craton: example of the Amsaga area (Rgueïbat rise). U-Pb and Sm-Nd evidence for crustal growth and recycling. Precambrian Research 90, 107-117, doi: 10.1016/S0301-9268(98)00044-8.

Praveen M.N., Ghosh B., Shrivastava H.S., Kumaran G.S., Roy S., Sisodiya D.S., 2005. Metamorphic mineral assemblages associated with sulphide mineralization in Betul Belt: A possible hydrothermal origin. In Proceeding volume of 1st Indian Mineral Congress "Showcasing the Indian Mineral Industry in the 21st Century", ISM, Dhanbad, India, 193-218. New Delhi: Allied Publishers.

Robert F. and Poulsen K.H., 2001. Vein formation and deformation in greenstone gold deposits. Society of Economic Geology Reviews 14, 111-155, doi: 10.5382/Rev.14.05.

Sabeima E. and Weal K.K.L., 2024. An Empirical Analysis of The Impact of the Exchange Rate on Exports: A Case Study of Mauritania. International Journal of Strategic Management and Economic Studies (IJSMES) 3, 1349-1366, doi: 10.5281/zenodo.13685687.

Schofield D.I., Horstwood M.S.A., Pitfield P.E.J., Crowley Q.G., Wilkinson A.F., Sidaty, H.C.O., 2006. Timing and kinematics of Eburnean tectonics in the central Rgueibat Shield, Mauritania. Journal of the Geological Society, London 163, 549-560, doi: 10.1144/0016-764905-097.

Schofield D.I., Horstwood M.S.A., Pitfield P.E.J., Gillespie M., Darbyshire F., O'Connor E.A., Abdouloye T.B., 2012. U-Pb dating and Sm-Nd isotopic analysis of granitic rocks from the Tiris complex: new constaints on key events in the evolution of the Reguibat Shield, Mauritania. Precambrian Research 204/205, 1-11, doi: 10.1016/j.precamres.2011.12.008.

Sibson R.H., Robert F., Poulsen K.H., 1988. High angle reverse faults, fluid pressure cycling and mesothermal gold-quartz deposits. Geology 16, 551-555, doi: 10.1130/0091-7613(1988) 016%3C0551:HARFFP%3E2.3.CO;2.

Sims J., 2019. Tasiast Project Mauritania National Instrument 43-101, Technical Report. Kinross Gold Corporation, 1-216. https://s2.q4cdn.com/496390694/files/doc_downloads/technical_reports/2019/Kinross-Tasiast-NI-43-101-Technical-Report-Oct-2019-FINAL.pdf (accessed 10 January 2020).

Taib Mowafa., 2019. The Mineral Industry of Mauritania, USGS Minerals Yearbook, (Advance Release), 59.1 pp.

Tan H., Shao Y., Liu Q., Zhang Y., Feng Y., Zhang Y., Shah S.A., 2022. Textures, trace element geochemistry and in situ sulfur isotopes of pyrite from the Xiaojiashan gold deposit, Jiangnan Orogen: Implications for ore genesis. Ore Geology Reviews 144, 104843, doi: 10.1016/j.oregeorev.2022.104843.

Taylor B.E., 2007. Epithermal gold deposits. Mineral Deposits of Canada: A synthesis of major deposit-types, district metallogeny, the evolution of geological provinces, and exploration methods: Geological Association of Canada, Mineral Deposits Division, Special Publication, 5, 113-139.

Trench A., Baur D., Ulrich S., Sykes J.P., 2024. Gold Production and the Global Energy Transition- A Perspective. Sustainability, 16, 5951, doi: 10.3390/su16145951.

Uytenbogaardt W. and Burke E.A.J., 1985. Tables for microscopic identification of ore minerals. Courier Corporation.

Zeine M., Soumary A., Cherif A., Mohamed M., Mouhamed I., Sow A., ... Medhioub M., 2019. Mineralogy, Petrography, and Geochemical Studies of the Greenstone Belt Rocks and the Associated Gold Mineralization of Aoueouat at Tasiast Mine, Mauritania. In Recent Research on Geomorphology, Sedimentology, Marine Geosciences and Geochemistry: Proceedings of the 2nd Springer Conference of the Arabian Journal of Geosciences (CAJG-2), Tunisia, 351-354. Springer International Publishing, doi: 10.1007/978-3-030-72547-1_75.

Vachette M. and Bronner G., 1973. Ages radiométriques Rb/Sr de 2900 et 2700 Ma des séries précambriennes de l'Amsaga et du Tiris, dorsale de Rgueïbat (Mauritanie).7éme Colloq. Int. Geol. Afr., Florence. Lab. Sci. Terre, St-Jérôme, Marseille, Série B, p. 147. (In French).

Villeneuve M., 2008. Review of the orogenic belts on the western side of the West African craton: the Bassarides,

Rokelides and Mauritanides. Geological Society, London, Special Publications, 297(1), 169-201, doi: 10.1144/SP297.8.
Weinberg R.F., Hodkiewicz P.F., Groves D.I., 2004. What control god distribution in Archeanterranes? Geology 32, 545-548, doi: 10.1130/G20475.1.
Witt W.K. and Vanderhor F., 1998. Diversity within a unified model for Archaean gold mineralization in the Yilgarn Craton of Western Australia: an overview of the late-orogenic, structurally controlled gold deposits. Ore Geology Reviews, 13, 29-64, doi: 10.1016/S0169-1368 (97)00013-9.